Journal of Hydrology: Regional Studies 1 (2014) 74–91

Contents lists available at ScienceDirect

Journal of Hydrology: Regional Studies

journal homepage: www.elsevier.com/locate/ejrh

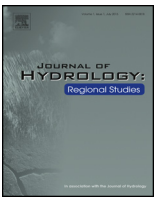

A simple, regionally parameterized model for predicting nonpoint source areas in the northeastern US

J.A. Archibald [a,*], B.P. Buchanan [a], D.R. Fuka [b], C.B. Georgakakos [a], S.W. Lyon [c], M.T. Walter [a]

[a] Department of Biological and Environmental Engineering, Cornell University, Ithaca, NY, USA
[b] Biological Systems Engineering, Virginia Polytechnic Institute and State University, Blacksburg, VA, USA
[c] Department of Physical Geography and Quaternary Geology, Stockholm University, Stockholm, Sweden

ARTICLE INFO

Article history:
Received 30 January 2014
Received in revised form 16 June 2014
Accepted 17 June 2014
Available online 2 August 2014

Keywords:
Watershed modeling
Nonpoint source pollution
Decision support tools
Phosphorus
Low parameter model
Agricultural runoff

ABSTRACT

Study Region: Ten watersheds in New York, New Jersey, and Pennsylvania, USA.

Study Focus: A three parameter model based on variable source areas (VSAs) that does not require calibration within the region, was developed and tested. The model maintains a lumped daily water budget, but distributes runoff spatially using a soil topographic index (STI). We used ten gauged watersheds across the region to establish the model parameters, and compared model predicted VSAs against shallow water table depth and surface soil moisture field measurements in three sites.

New Hydrological Insights for the Region: The model was able to correctly predict VSAs at all three monitoring sites, indicating that saturation-excess runoff is important in these watersheds. The pattern of error in the model suggests that lateral subsurface flow paths could be exerting an influence on overland runoff generation in a way that is not captured by a static STI. The model has potential to be used as part of a strategy to limit nonpoint source pollution from saturation-excess runoff dominated areas in the region, and has been incorporated into an online decision support tool in central NY (www.hsadss.bee.cornell.edu).

* Corresponding author. Tel.: +1 6072272096.
E-mail address: jaa78@cornell.edu (J.A. Archibald).

http://dx.doi.org/10.1016/j.ejrh.2014.06.003

1. Introduction

Many stakeholders are involved in addressing the persistent challenge of mitigating nonpoint source (NPS) pollution to protect receiving water resources, including scientists, farmers and landowners. For NPS pollutants that are transported disproportionately in runoff such as phosphorus (P), a useful strategy for minimizing water contamination would be to avoid polluting activities like manure fertilization in areas that are expected to generate overland runoff in the near future (Walter et al., 2000). In the northeastern US, storm runoff is most commonly generated in parts of the landscape prone to soil saturation; because these areas are dynamic in time and space they are commonly referred to as variable source areas (VSAs) (e.g., Dunne and Black, 1970). Several methods of predicting storm runoff locations in active agricultural lands have already been proposed (Agnew et al., 2006; Gburek et al., 2000; Marjerison et al., 2011). However, these methods generally ignore the dynamic behavior of VSAs, and this variability in time is arguably a more critical factor in contaminant transport. For example, McDowell and Srinivasan (2009) found that over 75% of P loading during a 20-month period came from three rainfall-runoff events. Such timing influence suggests that planners need to be concerned about hydrologically sensitive "moments" (HSM) in addition to hydrologically sensitive areas and avoid manure-fertilizer or other contaminant applications at these times and locations.

Concepts aligned with HSMs are gaining traction among decision makers and planners. Researchers studying P transport (e.g., Kleinman et al., 2011) and flood risk (e.g., Van Steenbergen and Willems, 2013) suggest using dynamic decision support systems (DSS) to deal with these issues. One example of this is the Wisconsin Manure Management Advisory System (DATCP, 2013). This is a dynamic agricultural nonpoint source DSS that addresses the timing component of runoff risk using weather forecasts to determine the potential risk of runoff on a watershed scale (on average 500 km^2). However, while knowledge of watershed-wide risk(s) is useful, it does not allow farmers or other land managers to target the highest-risk runoff-generating areas. The reality of farm manure management with finite-capacity manure storage facilities (e.g, manure lagoons) is that there are times when there is a pressing need to spread manure regardless of watershed-scale risk forecasts. Therefore, producers with limited manure storage are often left with little guidance about when and where runoff is predicted in order to prioritize risks at the farm scale.

In looking ahead to the next generation of watershed NPS-mitigation tools to provide farm and field-scale predictions of storm runoff risks, one challenge is developing a simple model with enough of a physical basis to correctly predict where and when storm runoff will be generated. Simplicity is important in models because excessive parameterization or calibration may be prohibitively complex for conservation planners, and could lead to over-calibration and a fundamental misrepresentation of the processes involved in runoff generation (e.g., Kirchner, 2006).

Considerable work has already been devoted to reducing the number of calibration parameters in a variety of watershed models (Pradhan and Ogden, 2010; Seibert, 1999). In order to do this, we often need to make some assumptions about the dominant underlying processes driving runoff in our watersheds of interest. For example, if we are primarily interested in the humid, well-vegetated northeastern USA, as is the case in this study, we can assume that saturation-excess is the main processes driving runoff and is expressed via shallow, lateral subsurface flows (a.k.a., interflows) that are a primary control on VSAs (Dunne and Black, 1970; Dunne and Leopold, 1978; Walter et al., 2003). From this standpoint, the goal of this study is to develop and test a minimally parameterized model for the northeastern USA. This model is designed to predict VSAs and hydrological response from readily obtainable watershed characteristics and forcing data that does not need to be calibrated. Specifically, we are interested in reducing the number of parameters and removing the need for watershed-specific calibration. To do this, we combine modeling concepts from STOPMODEL (Walter et al., 2002) and the Variable Source Loading Function (VSLF) model, which has been shown to work well in the northeastern US (Schneiderman et al., 2007). Although the model simulates stream discharge at the watershed outlet, our focus is on predicting the locations and timing of runoff generation.

A major advantage to STOPMODEL and VSLF is that they predict runoff generation in time and at spatial resolutions relevant to farmers (sub-field), which is our main goal in this application. As such, we extend a semi-distributed approach to watershed modeling that maintains a "lumped" watershed water balance and redistributes runoff based on soil topographic index (STI), as defined by Walter et al.

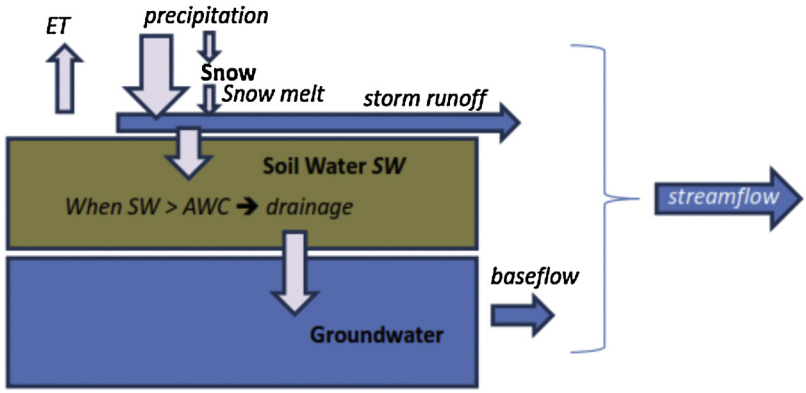

Fig. 1. Schematic of the lumped water budget model.

(2002). The STI is useful for pinpointing runoff generating landscape locations in humid regions (Lyon et al., 2004). In fact, Dahlke et al. (2013) successfully used this approach to calibrate a prototype of a DSS that is capable of using weather forecasts to predict saturated areas in a watershed. Here, we modify the Dahlke et al. (2013) model structure to create a simple VSA model that relies on three runoff parameters (a daily storage coefficient, and two parameters to determine the daily hydrograph shape). The resulting model is computationally efficient enough to be applied at large spatial scales and yet yields spatially explicit results that are useful for conservation planners tasked with targeting sub-field scale management practices. In addition to predicting when and where storm runoff will occur, this model uses open source coding (R-programming language, R Core Team, 2013) and information (e.g., USGS and USDA geographical information) in a manner that is easily applicable to web-based applications.

2. Conceptual model description

2.1. Water budget

The modeling approach adopted here is similar to that used by the early forms of TOPMODEL (Beven and Kirkby, 1979), STOPMODEL (Walter et al., 2002), and VSLF (Schneiderman et al., 2007) in which the soil- and ground-water budgets are maintained at the watershed scale (Fig. 1) while storm runoff is distributed according to topographic position within the watershed. The soil water budget that forms the backbone of the model was first proposed by Thornthwaite and Mather (1955). Daily modeled soil water and evapotranspiration (ET) are based on soil water status and potential evapotranspiration (*PET*):

$$SW_d = SW_{d-1} \exp\left(\frac{I_d - C_c PET_d}{AWC}\right) \quad \text{for} \quad I_d - C_c PET_d < 0 \tag{1a}$$

$$SW_d = SW_{d-1} + (I_d - C_c PET_d) - D \quad \text{for} \quad I_d - C_c PET_d \geq 0 \tag{1b}$$

$$D = SW_{d-1} + (I_d - C_c PET_d) - AWC \quad \text{for} \quad SW_{d-1} + (I_d - C_c PET_d) > AWC \tag{1c}$$

where SW_d is soil water depth on day d (mm), AWC is the watershed-wide average available water capacity of the soil (mm), I_d is water input on day d (rain + snow melt $- Q_d$) (mm), C_c is a generalized crop coefficient to scale PET under various effective vegetative covers (adopted from Shuttleworth, 1992), D is drainage to the groundwater (mm), and Q_d is storm runoff on day d (mm). Storm runoff is estimated using Eq. (2) (discussed in the next paragraph). The watershed-average AWC is calculated from the area-averaged AWC-percentage (mm water per mm of soil depth) and soil depths from the NRCS SSURGO database (NRCS, 2013). Daily PET is calculated using the Priestley–Taylor (1972) equation using daily maximum and minimum air temperature to estimate net radiation (Archibald and Walter, 2013). A similar method is used to model daily snow (Walter et al., 2005; Fuka et al.,

2012). Baseflow is modeled using a linear reservoir model adopting an average regional coefficient of 0.1 day^{-1} based on recession flow analysis of streams in the northeastern US (Frankenberger et al., 1999).

2.2. Storm runoff

Storm runoff is estimated using the SCS Curve Number equation (e.g., USDA-NRCS, 2004):

$$Q_d = \frac{{P_d}^2}{P_d + S_d} \tag{2}$$

where Q_d is runoff on day d (mm), P_d is the effective precipitation and/or snow melt (mm) for that day defined as rain plus snowmelt minus an initial abstraction – here we use initial abstraction = $0.05S_d$ for the Northeast (similar to Shaw and Walter, 2009) – and S_d is the storage parameter (mm), which changes in the model on a daily time-step based on average watershed soil water status, SW_d. Eq. (2) has been shown to be consistent with VSA hydrology (e.g., Steenhuis et al., 1995; Lyon et al., 2004; Schneiderman et al., 2007; Easton et al., 2008; Dahlke et al., 2012). However, the tabulated parameters for determining S are inconsistent with the VSA concept and do not work well in the Northeast (Shaw and Walter, 2009). Here we test a linear relationship between S_d and soil water deficit, $SWD_d = AWC - SW_d$.

2.3. Runoff hydrograph

Although simulating stream discharge is not the main objective of this model, the storm hydrograph is used to simulate storm water temporarily retained in the landscape after the storm is over, before ultimately draining to the river. In order to model runoff timing, we adapt a variation of the SCS synthetic unit hydrograph (USDA-NRCS, 2004) in which the hydrograph shape has a linear rising limb from the beginning of the storm to the time to peak, T_p, and an exponential falling limb characterized by a hydrograph shape parameter, b. We estimate T_p as an empirical, linear function of the time of concentration, T_c (Kirpich, 1940);

$$T_c = T_c \ \ (\mathrm{h}) = 0.00032L^{0.77}\left(\frac{\Delta E}{L}\right)^{-0.385}$$

where L is the longest flow path (m) and ΔE is the elevation change over L (m).

2.4. Spatial distribution of runoff

Modeled storm runoff is distributed across the watershed based on the approach proposed by Lyon et al. (2004) and used by Schneiderman et al. (2007). Briefly, runoff distribution follows the soil topographic index (STI) (Walter et al., 2002), which indicates the relative propensity of a particular location to saturate and generate runoff:

$$\lambda = \ln\left(\frac{a}{T\tan(\beta)}\right) \tag{3}$$

where λ is the soil topographic index [$\ln(\mathrm{day\,m^{-1}})$], a is the upslope contributing area per unit length of contour (m), T is transmissivity ($\mathrm{m^2\,day^{-1}}$) of the soil defined as the product of soil depth and saturated hydraulic conductivity, and β ($\mathrm{m\,m^{-1}}$) is the local slope (see Buchanan et al., 2013 for optimal ways to calculate these terms for northeastern US landscapes). The fractional area, A_f (dimensionless) of the watershed that is generating storm runoff (e.g., Steenhuis et al., 1995; Lyon et al., 2004) is given as:

$$A_f = 1 - \frac{{S_d}^2}{(P_d + S_d)^2} \tag{4}$$

We divide each watershed into wetness classes based on the quantiles of the STI (Eq. (3)); starting with the first wetness class corresponding to the wettest quantile of the watershed. We then calculate

Table 1
Characteristics of the 10 watersheds used in this study.

Watershed	USGS ID	Size (km^2)	Soil Depth (mm)[a]	*AWC* (mm)[a]
Biscuit Brook (NY)	01434025	9.6	500	50
Town Brook (NY)	01421618	37	1470	120
Neshanic River (NJ)	01398000	66	1140	160
Fall Creek (NY)	04234000	330	1990	110
Wappinger Creek (NY) (1999–2000)	01372500	470	1880	280
Beaver Kill (NY)	01420500	620	1200	100
Tunkhannock Creek (PA)	01534000	990	1950	170
Pine Creek (PA)	01548500	1600	1580	130
Raystown Branch Juniata River (PA)	01562000	2000	1120	120
Allegheny River (NY,PA)	03011020	4200	1560	160

[a] Area weighted averages based on SSURGO (USDA-NRCS).

the amount of soil water storage that is available in each wetness class using (Schneiderman et al., 2007):

$$\sigma_{w,d} = \left(S_d \sqrt{\frac{1}{1 - A_s}} - 1 \right) \tag{5}$$

where $\sigma_{w,d}$ (mm) is the daily effective soil water content for a particular wetness class, w, of the watershed and A_s is fractional area of the watershed of all wetness classes up to and including wetness class w (dimensionless, between 0 and 1) (for more details see Schneiderman et al., 2007). This method allows us to have different effective soil water contents throughout the watershed based on wetness classification; these values change over time based on S_d. The amount of storm runoff generated from each fractional area is then simply $P_d - \sigma_{w,d}$. Areas of a watershed where $\sigma_{w,d} \geq P_d$ do not generate storm runoff. This semi-distributed VSA model is included in the EcoHydRology package in R (Fuka et al., 2013b).

3. Methods

3.1. Determining regional model parameters

The conceptual model described here has three unknown parameters, S_d (Eq. (2)), and T_p and b, which characterize the storm hydrograph. All other parameters in the study were obtained independently from open source and commonly available data, e.g., soil properties (i.e., *AWC*, *T*) from the USDA-NRCS SSURGO or STATSGO databases, and watershed characteristics (i.e., a, tan(β), watershed area, etc.) determined from a USGS digital elevation model (DEM). We used 10 USGS-gauged watersheds in New Jersey (NJ), Pennsylvania (PA), and New York (NY) in the northeastern USA (Fig. 2) to develop methods for regionally estimating the unknown parameters. Watersheds varied in size from approximately 10 km^2 (Biscuit Brook, NY) to over 4000 km^2 (Allegheny River, NY, PA) (Table 1).

We used daily measurements of precipitation and maximum and minimum temperatures as inputs for the model (NOAA, 2013). Daily streamflow measurements at these sites were from the USGS (2013). Watershed characteristics determined by topography, average soil depth, average available water capacity, and latitude were from the USDA and the USGS (USDA-NRCS, 2013; USGS, 2013). These watersheds were used to develop regional relationships between a watershed-wide soil water deficit, SWD_d, and S_d. They were also used to determine a relationship between watershed size and topography, and T_p.

To develop a regional relationship for S_d, we identified 532 isolated events from all the watersheds considered. Because Eq. (2) is most accurate in larger precipitation events (USDA-NRCS, 2004), we only considered events with daily rain and/or snowmelt events that were at least 20 mm and associated with an isolated rise in the streamflow hydrograph. From these, we estimated the storm runoff using a one-pass baseflow separation filter (Lyne and Hollick, 1979) (Appendix A). We calculated S_d-values

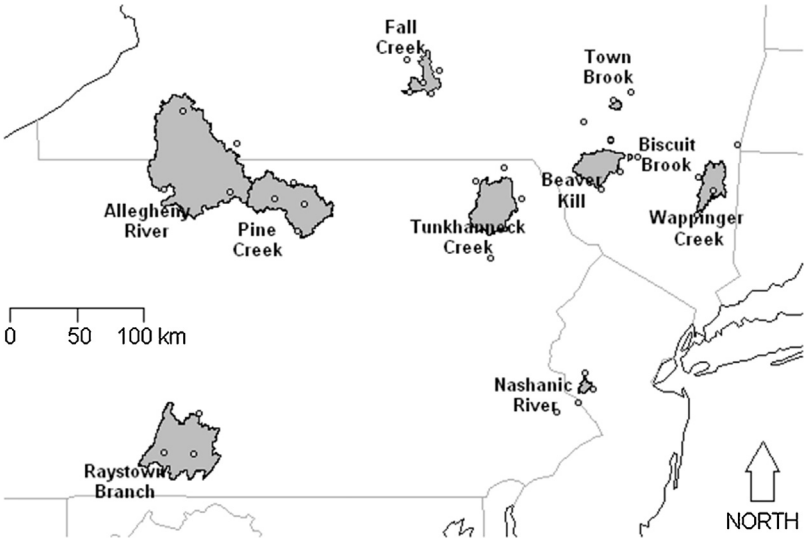

Fig. 2. Locations of the 10 watersheds used in this study, and the GHCN gauges used to model streamflow and saturation extent in the watersheds (open circles). Note, not all the gauges recorded precipitation and temperature data for all years between 1990 and 2010, so an average value of temperature and precipitation was recorded for each day using available data from the closest 2–4 gauges.

(by rearranging Eq. (2)) from these events using the technique described by Shaw and Walter (2009). We used Eq. (1) to estimate SW_d continuously to determine SWD_d, which we then correlated with the back-calculated S_d-values. We used the take-one-out methodology to ensure that no single watershed was biasing the S_d–SWD_d relationship.

To develop regionalized functions to describe the storm hydrograph, which has two parameters, T_p and b, we identified 214 well-defined events from the 10 watersheds. The criteria defining these events were: rain (+snow melt) > 10 mm and no days with more than 2 mm for the two preceding and the five following days. These criteria allowed us to balance identifying many hydrographs while minimizing the impacts of rain and snow melt before and after an event on the hydrograph shape. The b parameter determines the overall shape of the runoff hydrograph, and for this study we found that a constant value of 4.5 allowed us to reproduce the overall runoff pattern for all watersheds after manual calibration. Based on the proportion of runoff that reached the outlet on each of the 5 days following a rain or snow melt event, we were able to determine a best-fit T_p which minimized the root-mean-square error between the predicted and observed runoff shape (see Appendix A for further details). We used the take-one-out approach to evaluate the degree to which any one watershed influenced the relationships between the best-fit T_p and T_c.

3.2. Model application

We performed three independent tests on our model: (1) we used a leave-one-out approach to see how well our model would predict the hydrograph of a watershed that was not used to determine the regional model parameters, (2) we compared our predicted storm runoff locations to shallow water table measurements, and (3) we compared our predicted storm runoff locations to measured soil moisture.

3.2.1. Test 1: hydrograph analysis

To understand how the model would perform in ungauged watersheds, we considered the recalculated relationships between S and SWD_d and between T_c and T_p, determined by systematically

Table 2
S_{min} and C_1 are the intercept and slope of the relationship between S_d and SWD_d (Eq. (6)) calculated excluding values from each watershed; C_2 and C_3 are the coefficients used in the linear equation relating T_c to T_p (Eq. (7)) when excluding data for each watershed and $T_{p,TOO}$ is the time to peak calculated (Eq. (7)) using the C_2 and C_3 based on the other nine watersheds.

Watershed	Period modeled	S_{min} (mm)	C_1	C_2	C_3 (h)	T_c (h)	$T_{p,TOO}$[a] (h)
Biscuit Brook	1990–2010	78	3.4	0.32	3.6	0.53	3.8
Town Brook	1997–2010	82	3.4	0.33	3.5	1.4	4.0
Neshanic River	1990–2010	86	3.3	0.31	3.8	2.8	4.7
Fall Creek	1990–2010	84	3.5	0.33	3.5	8.7	6.4
Wappinger Creek	1999–2010	82	3.4	0.33	3.1	8.9	6.0
Beaver Kill	1990–2010	80	3.4	0.33	3.5	7.3	5.9
Tunkhannock Creek	1990–2010	82	3.5	0.33	3.3	8.4	6.1
Pine Creek	1990–2010	81	3.5	0.33	3.5	14	8.2
Raystown Branch	1990–2010	83	3.4	0.28	3.6	21	9.5
Allegheny River	1990–2010	81	3.5	0.46	2.6	30	16
All watersheds		82	3.4	0.33	3.4		–

[a] T_p determined using the take-one-out approach. Note that these are different from the best-fit T_p values shown in Fig. 5.

excluding one watershed in a leave-one-out approach (Arlot and Celisse, 2010). We then used these relationships to model the excluded watershed and compare the predicted and observed discharge hydrographs; note, in the earlier part of this paper we were only investigating how sensitive the parameters were to any one watershed and here we are evaluating model performance. The values of the coefficients for the relationships between measured and model parameters when excluding each watershed are reported in Table 2.

Modeled results were compared to USGS daily streamflow measurements at each location. In addition to the Nash-Sutcliffe efficiencies (NSE), we determined the ratio of the root mean square error to the standard deviation of observed streamflow (RSR) and the percent bias (PBIAS) for each watershed (Nash and Sutcliffe, 1970). Moriasi et al. (2007) proposed that a model is satisfactory if NSE > 0.50, RSR < 0.70, and has an absolute PBIAS < 25%. We also calculated NSE on an event basis, where runoff events were initiated by a 1 day rise in the observed USGS hydrograph after at least 2 days of decreasing flows.

3.2.2. Test 2: water table analysis

We created a LIDAR-derived STI (Fig. 3) for comparison to water table height measurements from Town Brook Watershed, using: (i) a 3 m LIDAR-derived DEM from the NY Department of Environmental Protection (DEP), (ii) maximum triangular slope (Tarboton, 1997), (iii) the Multiple Triangular Flow Direction method (Seibert and McGlynn, 2007) as per Buchanan et al. (2013). We then binned STI values into equal-area wetness classes, such that low-numbered wetness classes are wetter areas (large STI values) and high wetness classes signify dry areas of the watershed (low STI values). This allowed us to assign a location as “wet” or “dry” during a storm event based on the saturated extent predicted by the model.

Lyon et al. (2006) collected 6 months of 15-min interval shallow water table measurements in a 2 ha near-stream region in the Town Brook, NY watershed (inset, Fig. 3). We used maximum daily water level measured in 18 wells (Lyon et al., 2006) recorded via WT-HR 500 capacitance probes (TruTrack, Inc., New Zealand). We ran the watershed model using precipitation data measured on-site and temperature data from Delhi, NY. On days when runoff was predicted, we divided the wells into “wet” locations where our model predicted runoff generation and “dry” locations where our model predicted no runoff generation to compare water table depths between groups.

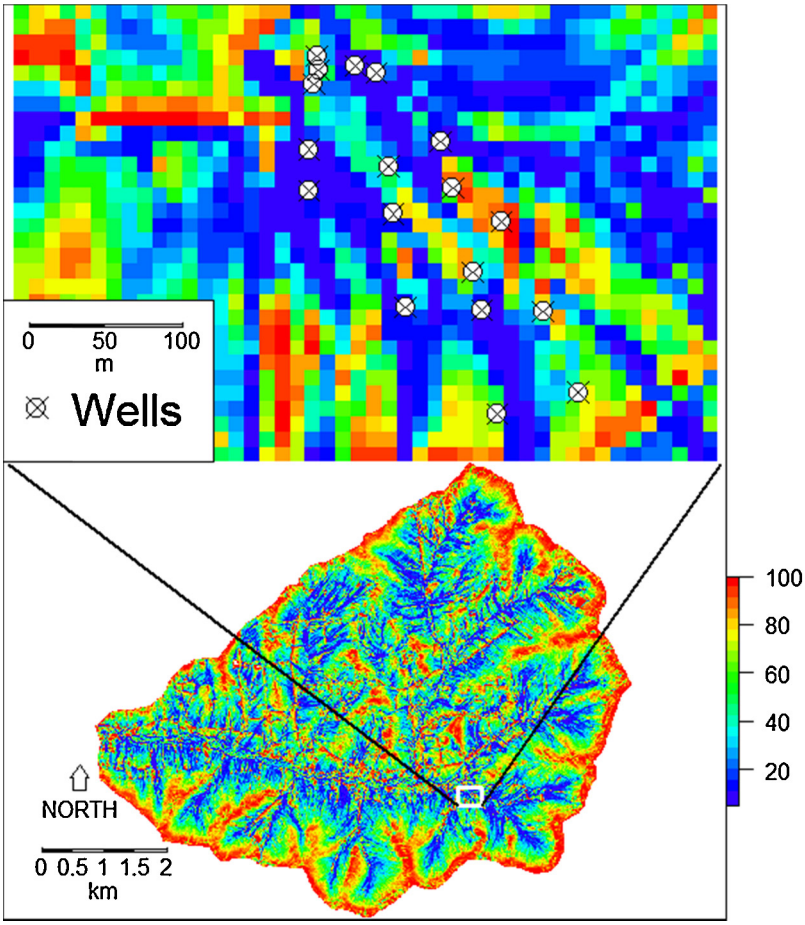

Fig. 3. Town Brook watershed broken into 100 equal area wetness classes based on a 3 m LIDAR DEM. Wet areas are blue and have a low number wetness class, while dry areas are labeled red and have high wetness class values (see color ramp). The top map shows the locations of the shallow water table wells used in this analysis (Lyon et al., 2006).

3.2.3. Test 3: soil moisture analysis

Volumetric soil moisture measurements were taken at two field sites in Fall Creek and Cascadilla Creek watersheds (near Ithaca, NY) over the course of Fall 2012 and Spring 2013 (Fig. 4). Measurements were taken in triplicate using a TDR probe over a range of wetness classes (Buchanan et al., 2013). We assigned a wetness class to each sampling location using a 3-m LIDAR derived STI value (same method as in Test 2). For each measurement date, we modeled the extent of saturated areas in the contributing watershed that were predicted to generate runoff on that particular date. Using this breakdown, we assigned each soil moisture measurement point a predicted value of "wet" and "dry" based on whether the model predicted the point to be generating runoff or not, respectively. This was compared to the soil moisture status of these wet and dry locations. The number of wet and dry locations changed on each measurement date, depending on the extent of saturation predicted for that day. We estimated the porosity of the soil as 53% assuming minimal organic matter using the bulk density reported in the USDA SSURGO data set (USDA-NRCS, 2013).

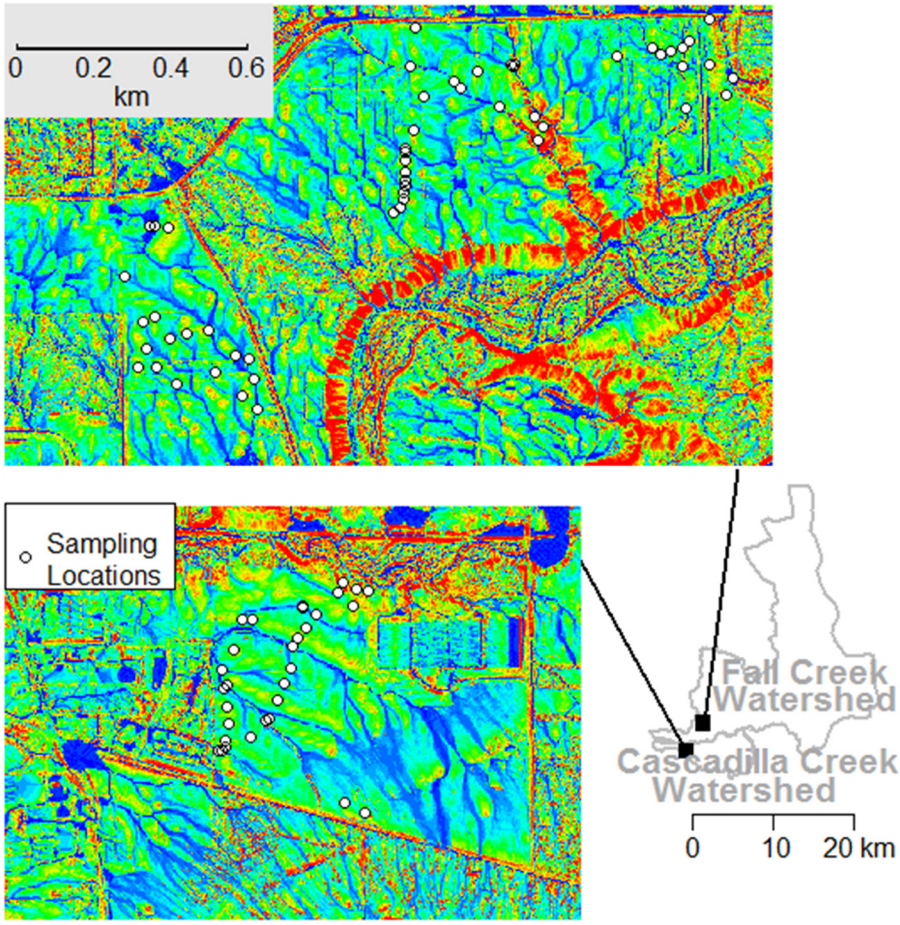

Fig. 4. Wetness class maps of the soil moisture measurement sites in Fall Creek and Cascadilla Creek watersheds. Blue areas have a low wetness class value and are most likely to generate runoff, while red areas have high wetness class values and are expected to remain dry (see color ramp in Fig. 3). *Note*: the linear wet and dry features represent the effects of roads and roadside ditches (i.e., linear blue areas are road ditches and red linear features are the downslope, drying-out effects due to the ditches).

4. Results

4.1. Determining regional model parameters

4.1.1. Calculating the curve number S (S_d) from a watershed-wide soil water deficit (SWD_d)

We found there was a significant ($p < 0.001$) linear relationship between S_d and SWD_d, which is represented by Eq. (6) and overall coefficients reported in Table 2.

$$S_d = S_{\min} + C_1(SWD_d) \tag{6}$$

We recalculated this relationship by excluding data from each watershed individually, and found that the relationship remained significant at the $p < 0.001$ level for each watershed excluded, with the intercept, $S_{\min}$, varying between 78 and 86 mm, and the slope, C_1, varying between 3.3 and 3.5 (Table 2 and Fig. 5). This suggests that we can use Eq. (6) to determine S_d from SWD_d directly, without needing

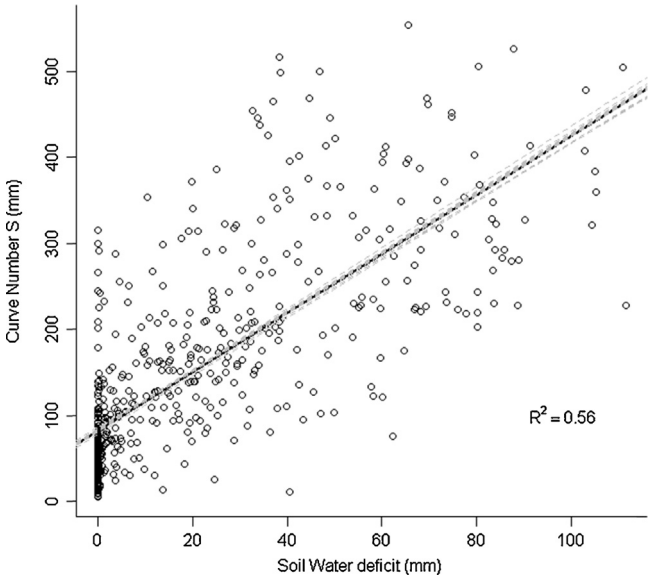

Fig. 5. Observed S_d verses soil water deficit (SWD_d) on the day preceding runoff initiation. The dashed gray lines are the relationships found when removing one watershed at a time from the 10-watershed dataset. Intercept varied between 78 and 86, slope between 3.3 and 3.5 (Table 2); the relationship was always significant, p-value <0.001 (even when all 110 points with SWD_d = zero are removed).

to calibrate unique coefficients for individual watersheds, i.e., we can use the average values for $S_{\min}$ and C_1.

4.1.2. Estimating the hydrograph shape using watershed characteristics

The best-fit T_p values were well correlated ($R^2 = 0.80$, $p < 0.01$) to T_c (Fig. 6), and we determined a linear relationship that allows us to estimate T_p based on T_c:

$$T_{p,c} = C_2 T_c + C_3 \tag{7}$$

where $T_{p,c}$ is the calculated time to peak (h), C_2 is a fitted slope of 0.33 (unitless), and C_3 is the fitted intercept of 3.4 (h). We recalculated C_2 and C_3 using the leave-one-out method (Fig. 6); R^2 varied between 0.77 and 0.88 for the various combinations of nine watersheds, C_2 varied between 0.28 and 0.46, and C_3 varied between 2.6 and 3.76 h (Table 2).

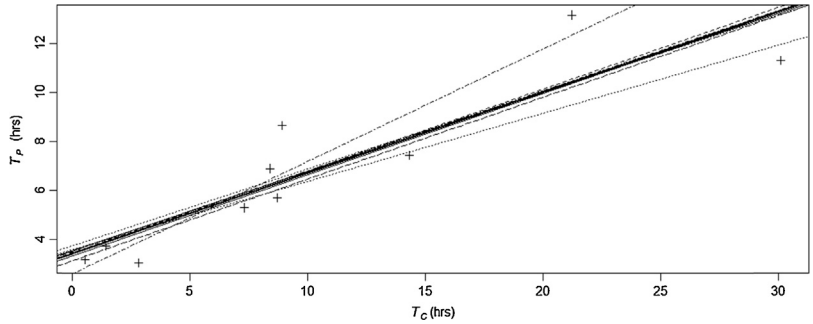

Fig. 6. Relationship between the best fit-determined T_p and T_c calculated for each watershed. The dashed lines are the relationship recalculated by dropping each watershed from the data. This take-one-out approach is useful for applying the relationship for each watershed without including data taken from that particular watershed.

Table 3
Model results for the 10 USGS gauges used in this study based on a take-one-out approach. Daily NSE values in parentheses are during periods that include additional precipitation gauges inside the watershed (if applicable). RSR is the ratio of the root mean square error to the standard deviation of observed streamflow, and PBIAS is the percent bias (Moriasi et al., 2007). The average gauge distance from watershed was calculated by assigning a distance of zero for all gauges inside the watershed, and using the dist2Line function in the R-package geosphere (Hijmans et al., 2012) to calculate the minimum distance from a gauge to the closest point along the watershed's boundary.

Watershed	Event NSE	Daily NSE	RSR	PBIAS (%)	Average gauge distance from watershed (km)
Biscuit Brook	0.71	0.55	0.68	−3.9	14
Town Brook	0.64	0.50	0.70	7.2	15
Neshanic River	0.48	0.18	0.90	−33	8
Fall Creek	0.72	0.67	0.58	−1.2	2
Wappinger Creek	0.56	0.57 (0.64)	0.66	−17	5–6
Beaver Kill	0.59	0.61	0.63	−4.6	5
Tunkhannock Creek	0.55	0.67	0.58	−17	8
Pine Creek	0.66	0.67	0.57	−6.9	0.4
Raystown Branch	0.56	0.56	0.67	−16	0.5
Allegheny River	0.62	0.64 (0.68)	0.60	5.5	0.4–2
Average	0.61	0.56	0.66	−9.8	3.5

4.2. Model application

4.2.1. Test 1: hydrograph analysis

Modeled flow compared reasonably well to observed flow at nine of the 10 gauges (Table 3 and Fig. 7). These values improved during time periods when there was a rain gauge inside the watershed. For example, the Wappinger Creek NSE improved to 0.64 from 0.57 for daily flow after 2004, when a NOAA gauge is active inside the watershed. Using these measures, the model appears acceptable in nine of the 10 watersheds, although it fails in the Neshanic River, NJ in all three metrics. Interestingly, event flow analyses showed better performance relative to daily for the small watersheds and no change or worse performance for the larger watersheds.

4.2.2. Test 2: water table analysis

Over the 6-month period of observations in Town Brook watershed, the model predicted 16 occurrences of overland runoff. During 15 of those events, the median water table depth for locations estimated as being "wet" was less than 100 mm from the soil surface, while the median dry wells remained at or below a depth of 100 mm during all events (Fig. 8). This corroborates previous findings that overland runoff in the Northeast is initiated once the water table is within approximately 100 mm of the surface (Lyon et al., 2006; Dahlke et al., 2012).

Over the course of the 16 events, we compared 288 separate predictions of wet or dry conditions to field measurements. In 18 cases (6%), we predicted a well to be wet when the water table at that location was below 100 mm and in 55 (19%) cases we predicted a well to be dry when the water table depth was within 100 mm of the soil surface. The remaining 215 (75%) predictions correctly identified a location as wet or dry based on modeled results. On days when no runoff was predicted, the average depth to the water table of all wells was 240 mm.

4.2.3. Test 3: soil moisture analysis

At the Fall Creek site, four out of the 13 measurement dates were predicted to have saturated areas contributing to storm runoff. In three of the four dates, the median volumetric soil moisture reading in the modeled wet locations was above saturation (i.e., $\geq$53%), while dry locations had median values below saturation (Fig. 9, top). On the date that the "wet" wells were below the saturated value (June 26, 2013), the observed streamflow at the outlet did not show a discernible rise in the hydrograph, highlighting the difficulty in correctly modeling small storm runoff events. The Cascadilla Creek site only had one instance of measurements being taken in locations predicted to be wet, and on this date, the wet sites had a median soil moisture status above saturation (Fig. 9, bottom).

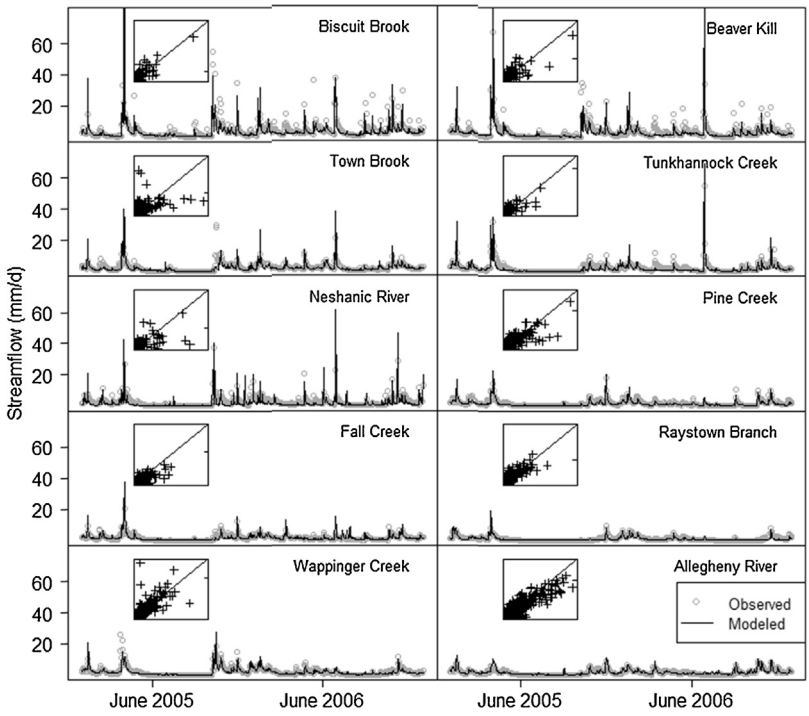

Fig. 7. Observed and modeled streamflow during the 2-year period between 2005 and 2006. Observed flow is shown as gray open symbols, while modeled flow is the black line. Inset scatter plots are modeled flow on the vertical axis against measured streamflow on the horizontal axis, the line shows the 1–1 relationship.

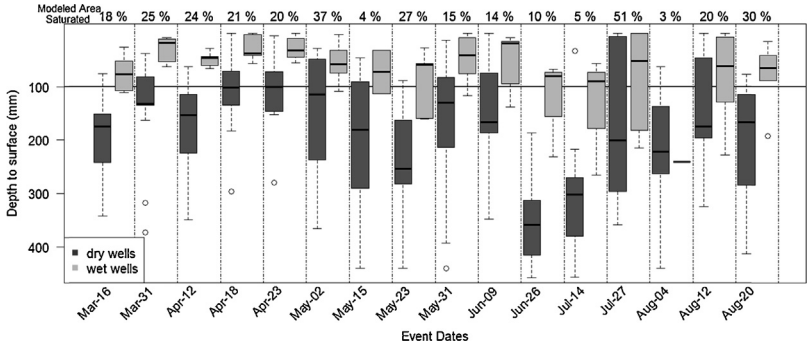

Fig. 8. Water table depths in the 18 wells in Town Brook Watershed during runoff events, categorized by model predictions of wet area extent distributed using a 3 m LIDAR-derived STI. The numbers along the top signify the percentage of the watershed that was predicted to be wet for that event. The cutoff line between dry and wet wells is 100 mm, with only one occurrence of the median occurring below, on August 4th.

5. Discussion

The model presented here shows promise as a simple tool allowing for spatial prediction of saturation-excess runoff locations in the northeastern US. Areas that were predicted to generate overland runoff had higher average soil moisture status and an elevated water table compared to areas modeled to be dry within three watersheds. As such, this model may serve as an effective screening tool for identifying sub-field scale runoff source areas or VSAs. It is particularly important to identify

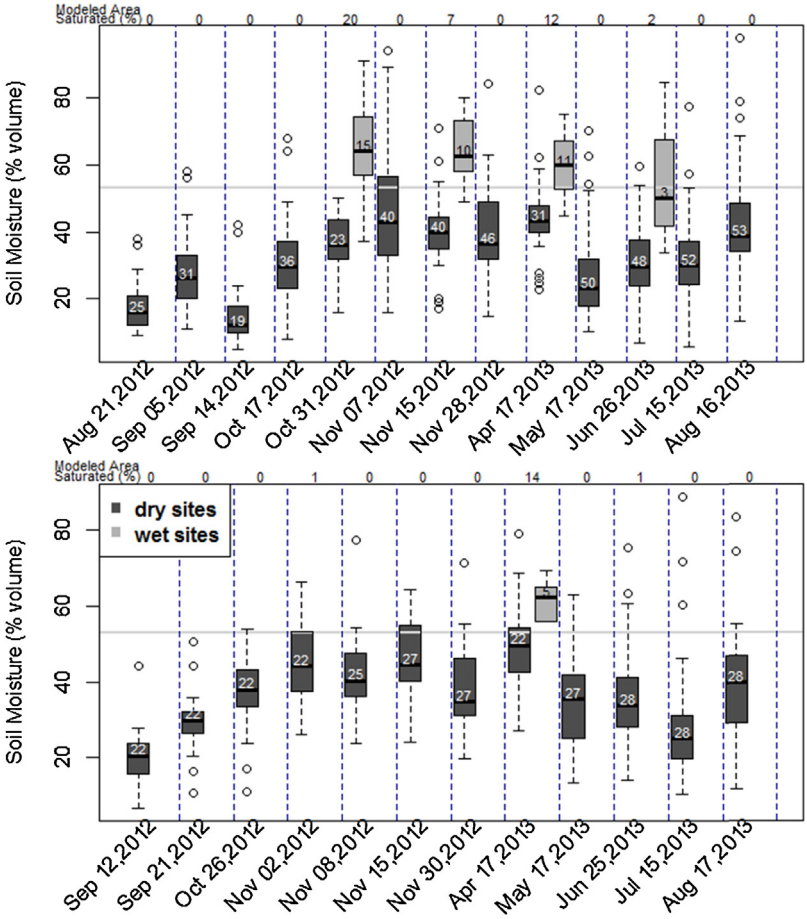

Fig. 9. Soil moisture readings at the Fall Creek (top), and Cascadilla Creek (bottom) sites. On the days that runoff was predicted, sites were categorized as "wet" if their STI value put them within the wettest modeled percentage of watershed predicted to be contributing to runoff on that day. Light gray box-plots are measurements at locations that were labeled as wet by the model, dark gray boxes are locations that were predicted to be dry. The numbers along the top of the graph are the percentage of the watershed predicted to be contributing to runoff on that day. The numbers above the median line in the boxes are the number of measurements. The gray horizontal line is the estimated porosity of the soil, 53%, and we assume that measurements above this signify saturation.

these VSAs when modeling contaminants that are disproportionately transported in overland flow, such as P.

Further, the model correctly identified dry locations and periods, indicating the model's ability to reflect HSMs and potential runoff source area variability. This has important implications for management as it indicates that this approach could be implemented as a real-time, spatiotemporally dynamic runoff risk tool at the sub-basin and sub-field scale (similar to Dahlke et al., 2013). This would contrast with other real-time watershed tools, such as the Wisconsin Manure Management Advisory System, that advise users of risks on a watershed-wide basis (DATCP, 2013). These prediction tools would be most useful in the context of trying to minimize phosphorus or sediment losses in runoff.

It is instructive to look at the two watersheds where model performance was the worst, Neshanic River and Town Brook watersheds, as it allows us to use the model as a hypothesis testing tool. Both of these watersheds are small and have no internal rain gauges and, thus, the amount of rain we are assuming is occurring in the watershed may be incorrect. Fuka et al. (2013a) demonstrate that when a

weather gauge is greater than 10 km from a small basin, even a short term weather forecast may result in better model performance relative to using the weather station. In particular, the Neshanic River streamflow response was poorly modeled and this could also indicate that some of our underlying assumptions about runoff processes in this watershed are incorrect, i.e., infiltration excess runoff could have a larger impact in this basin because of its relatively large urban footprint.

In the Town Brook site, there were a number of instances when we incorrectly categorized wells during runoff events. Interestingly, each well was mis-categorized at least once in the 18 runoff events. This is instructive, because it suggests that we are not so much mis-categorizing some wells entirely (which would be caused by an inaccurate STI), but instead that the water table dynamics are more variable than we are able to capture with this simple model. This is consistent with findings from Harpold et al. (2010) who, using an end-member mixing analysis, determined that lateral preferential flow paths were redistributing water beyond what is predicted by VSA models.

One limitation of this semi-distributed model is that the static nature of the STI classifications does not allow us to distinguish between upland wet sites and the lowland sites directly contributing to tributaries. We expect upland areas to show a much flashier response to precipitation inputs than lowland areas when their STI values are similar. Archibald (2010) found that water tables in lowland wetlands remained high, within 100 mm of the soil surface, for 7 months of the year, while upland wetland water tables in locations with similar STI values became saturated and drained within a few days of a rain event throughout the year. The next generation of runoff prediction tools could move away from the lumped approach and distribute runoff over the landscape on a daily basis; however, if the end goal is a web-based mapping tool, this will require addressing the challenges of higher computer processing power and daily creation of unique map layers.

The empirical relationships developed here for the two variable model storm runoff parameters (S_d, T_p) appear to be regionally generalizable within the context of rural watersheds. We suggest this model as a potential tool for predicting flows in ungauged watersheds in the northeastern US. A beta website using the methodology described here is available for the Owasso Lake Watershed in upstate NY (Cornell Soil and Water Lab, 2013).

6. Conclusions

This study developed and applied a parsimonious semi-distributed hydrologic model (Lumped VSA model) across a variety of watersheds and field sites. The model performed well over multiple scales of validation and was able to simulate both watershed-scale streamflow response and groundwater table and soil moisture dynamics at the sub-field scale. Given the relatively simple model structure, transparent theoretical underpinnings and minimal calibration, the model is useful not only for predicting hydrologic response but also for testing its underlying assumptions about the dominant hydrological processes. As the model yields predictions of runoff generating zones, it forms the basis for a decision support tool for identifying critical runoff source areas in combination with "hydrologically sensitive moments" that have a high potential for targeted management practices. It is important to note that users interested in using this model should verify that saturation-excess runoff processes are important in their region. If not, it is likely that a simpler approach of avoiding polluting activities in areas that have low infiltration capacities or during times of the year when high intensity storms are expected would be more effective.

In addition, model predictions are limited by the resolution of the DEMs underlying the STI maps. Small-scale flow paths such as ditches can radically alter surface water dynamics, but are not always identified in STIs created from USGS 10 m DEMs. Instead, LIDAR–derived STIs are more likely to capture small scale spatial wetness patterns (Buchanan et al., 2013). Additionally, we expect tile drains to prevent overland runoff in areas the model will predict to be wet. However, because tile drains create an alternate rapid pathway for water, they also have potential to transport P and other pollutants from agricultural fields (Geohring et al., 2001), and so the prediction of runoff generation in these areas could be a useful indication of another rapid transport mechanism to stream outlets.

Acknowledgments

Funding for this research came from the USDA through a NIFA Land Grant number 2012-67019-19434. We gratefully acknowledge the USGS, USDA, NOAA data sources used in this study, and the R-project and associated packages that greatly helped in the analysis of the data (R-Project, including the packages RSAGA, rgdal, maps, PBSmapping, raster, and GISTools).

Appendix A.

The runoff hydrograph

The synthetic hydrograph used here has a linear increase to peak followed by an exponential decrease (Fig. A.1) and is defined by two parameters, time to peak, T_p, and a shape parameter, b, which determines the height of the peak and the length of the tail with respect to T_p.

$$q = \begin{cases} \dfrac{2t}{(1+b){T_P}^2}, & t < T_P \\ \dfrac{2e^{-2(t-T_P)/(bT_P)}}{T_P(b+1)}, & t \geq T_P \end{cases} \tag{A.1}$$

where q is the instantaneous runoff fraction (time^{-1}), and t is time since runoff began (same units as T_p, here, h). Because we are modeling runoff on a daily time-step, we use the integral of Eq. (A.1) with respect to t to determine the cumulative runoff fraction:

$$\frac{Q}{Q_{tot}} = \begin{cases} \dfrac{t^2}{{T_P}^2(1+b)}, & t < T_P \\ 1 - \dfrac{be^{-\dfrac{2(t-T_P)}{bT_P}}}{b+1}, & t \geq T_P \end{cases} \tag{A.2}$$

where Q is runoff depth at time t (defined as the time since runoff began, h), Q_{tot} is the total runoff depth for this runoff event, b is the shape parameter of the curve (dimensionless). Eq. (A.2) can take very different shapes depending on the length of T_p in relation to the daily time step (Fig. A.1).

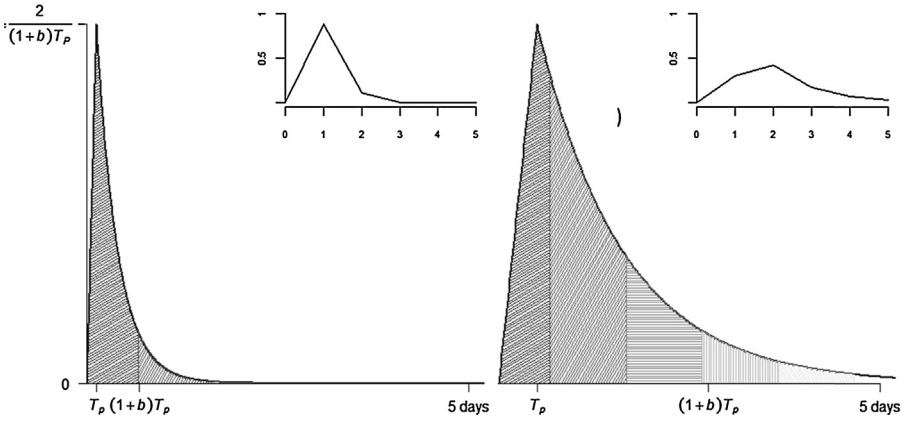

Fig. A.1. Integrating the continuous hydrograph over a daily time step allows us to see the daily runoff pattern (insets). Watersheds with a quick response time as in (a) (T_p = 3 h), will see most of the runoff generated from a single storm reach the outlet on the first day. A longer T_p as in (b) (T_p = 12 h), creates a more dampened runoff pattern. To handle the timing mismatch between USGS gauges (being from midnight to midnight) and most NOAA gauges (approximately 8–8 a.m.), we summed the first 16 h of the hydrograph for the first day of runoff and summed the full 24-h periods for subsequent days.

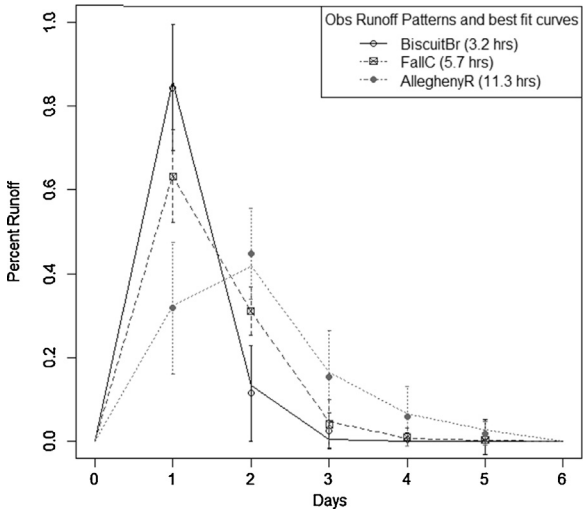

Fig. A.2. Observed (symbols; error bars represent the standard deviation from the mean of all events for that watershed) and best-fit (lines) daily runoff patterns for three watersheds (the smallest, an intermediate, and largest area watersheds). The best-fit T_p values, indicated in parentheses, were determined by minimizing the RMSE between the observed runoff pattern and the runoff pattern calculated from Eq. (A.2) by varying T_p.

Estimating T_p and b

We calculated the event-based daily runoff fraction for each watershed over the 5-day period following isolated rain events by dividing the amount of runoff from a particular day following rain input by the total runoff over the 5-day period. The daily runoff fractions were then averaged over all events for each day following runoff initiation. From these, we determined the average T_p for each watershed by minimizing the root mean square error (RMSE) between the 5-day runoff patterns observed with the expected runoff breakdown determined by Eq. (A.2). A representative subset of the resulting best-fit runoff patterns and the observed runoff patterns are shown in Fig. A.2.

T_p was not constant across watersheds. We investigated two potential predictors of T_p: T_c and watershed area. In calculating T_c, we determined the longest flowpath, L, using ArcHydro's longest flowpath tool with 10 m DEMs from the USGS (ESRI, 2009; USGS, 2013). The relationship between T_c and T_p are reported in Section 4.1.2. The linear relationship found between T_p and watershed area ($T_{p,A} = 0.002A + 4.7$; A = watershed area, km^2) was also significant, with $R^2 = 0.62$ and could be useful when information on longest flow path is not easily obtainable.

We also compared the observed cumulative runoff fraction against time since storm runoff began normalized by the calculated T_p (i.e., $T_{p,c}$, Eq. (7), with $C_2 = 0.33$ and $C_3 = 3.4$ h) (Fig. A.3). Normalizing time since runoff began (t) by $T_{p,C}$ allows all observations to be compared against the predicted cumulative runoff curve (Eq. (A.2)). The observed runoff fractions from all watersheds compared well with the predicted runoff pattern, with an R^2 of 0.94, and RMSE of 0.05.

Choosing runoff events for SWD_d–S_d relationship determination.

The rainfall/snowmelt-runoff events used to determine the coefficients in Eq. (6) were chosen with the following requirements. The rain or snowmelt triggering the event was at least 20 mm and the rain or snowmelt within 2 days before and 4 days after this trigger was less than 10 mm. We calculated the runoff that occurred after that rainfall/snowmelt trigger by using a one-pass baseflow separation filter (Lyne and Hollick, 1979) and summing the quickflow that occurred after the rain event until it returned to zero or up to 4 days of runoff, which-ever was shorter. This window was chosen to maximize the amount of events that could be included in the analysis, while minimizing the impact of

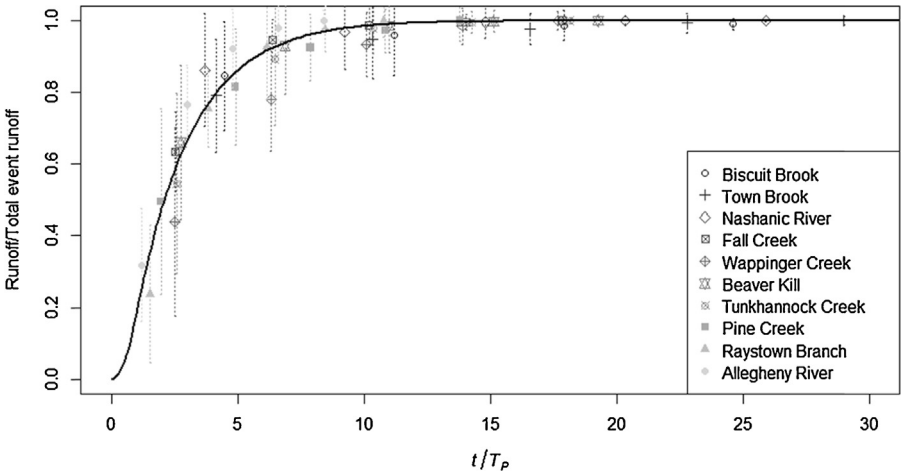

Fig. A.3. Observed cumulative runoff proportion vs. time since runoff began (t) normalized for $T_{p,C}$ (Eq. (7)) for all 10 watersheds (symbols); $R^2 = 0.94$ and RMSE = 0.05 (fraction of total runoff, unitless). Symbols are measured runoff fractions, and error bars on the observations indicate one standard deviation from the mean. The smooth curve represents the expected runoff fraction based on equation.

additional runoff from previous or subsequent events. Our runoff hydrograph analysis (Appendix A) indicated that at least 97% of the runoff following an event reached the outlet in these 10 watersheds within a 4-day period. We also removed events which had runoff values greater than 10% of baseflow before the precipitation event, and if no streamflow peak occurred within 4 days of runoff starting to further ensure that the relationship was not influenced by other storm events. These criteria further allowed us to exclude events that were likely to have been influenced by runoff from other rain or snowmelt events.

References

Agnew, L.J., Lyon, S., Gérard-Marchant, P., Collins, V.B., Lembo, A.J., Steenhuis, T.S., Walter, M.T., 2006. Identifying hydrologically sensitive areas: bridging the gap between science and application. J. Environ. Manage. 78, 63–76.

Archibald, J.A., Walter, M.T., 2013. Comment on "Assessing temperature-based PET equations under a changing climate in temperate, deciduous forests by Shaw and Riha". Hydrol. Process. 27 (24), 3511–3515, http://dx.doi.org/10.1002/hyp.9971.

Archibald, J.A., MS Thesis 2010. Dissolved Phosphorus in Shallow Groundwater. Cornell University.

Arlot, S., Celisse, A., 2010. A survey of cross-validation procedures for model selection. Stat. Surv., 40–79, http://dx.doi.org/10.1214/09-SS054.

Beven, K.J., Kirkby, M.J., 1979. A physically based, variable contributing area model of basin hydrology/Un modèle à base physique de zone d'appel variable de l'hydrologie du bassin versant. Hydrol. Sci. Bull. 24, 43–69.

Buchanan, B.P., Fleming, M., Schneider, R.L., Richards, B.K., Archibald, J., Qiu, Z., Walter, M.T., 2013. Evaluating topographic wetness indices across central New York agricultural landscapes. Hydrol. Earth Syst. Sci. Discuss. 10, 14041–14093.

Cornell Soil and Water Lab, 2013. HSA-DSS Tool [WWW Document]. http://hsadss.bee.cornell.edu/OwascoLake/ (accessed 23.11.13).

Dahlke, H., Easton, Z., Fuka, D., Walter, M., Steenhuis, T., 2013. Real-time forecast of hydrologically sensitive areas in the Salmon Creek Watershed, New York State, using an online prediction tool. Water 5, 917–944.

Dahlke, H.E., Easton, Z.M., Walter, M.T., Steenhuis, T.S., 2012. Field test of the variable source area interpretation of the curve number rainfall-runoff equation. J. Irrig. Drain. Eng. 138, 235–244.

DATCP, 2013. Runoff Risk Advisory Forecast [WWW Document]. Wis. Manure Manag. Advis. Syst http://144.92.93.196/app/events/runoff_forecast (accessed 14.10.13).

Dunne, T., Black, R.D., 1970. Partial area contributions to storm runoff in a small New England watershed. Water Resour. Res. 6, 1296–1311.

Dunne, T., Leopold, L.B., 1978. Water in Environmental Planning. W.H. Freeman, New York, NY.

Easton, Z.M., Fuka, D.R., Walter, M.T., Cowan, D.M., Schneiderman, E.M., Steenhuis, T.S., 2008. Re-conceptualizing the Soil and Water Assessment Tool (SWAT) model to predict saturation excess runoff from variable source areas. J. Hydrol. 348 (3–4), 279–291.

ESRI (Environmental Systems Resource Institute), 2009. ArcMap 9.2. ESRI, Redlands, California.

Frankenberger, J.R., Brooks Erin, S., Walter, M., Todd Walter Michael, F., Steenhuis Tammo, S., 1999. A GIS-based variable source area hydrology model. Hydrol. Process. 13, 805–822.

Fuka, D.R., Easton, Z.M., Brooks, E.S., Boll, J., Steenhuis, T.S., Walter, M.T., 2012. A simple process-based snowmelt routine to model spatially distributed snow depth and snowmelt in the SWAT Model 1. J. Am. Water Resour. Assoc. 48, 1151–1161.
Fuka, D.R., Walter, M.T., MacAlister, C., Degaetano, A.T., Steenhuis, T.S., Easton, Z.M., 2013a. Using the climate forecast system reanalysis as weather input data for watershed models: using CFSR as weather input data for watershed models. Hydrol. Process., http://dx.doi.org/10.1002/hyp.10073.
Fuka, D.R., Walter, M.T., Archibald, J., Steenhuis, T.S., Easton, Z., 2013b. EcoHydRology: A Community Modeling Foundation for Eco-Hydrology. http://cran.r-project.org/web/packages/EcoHydRology/EcoHydRology.pdf
Gburek, W.J., Sharpley, A.N., Heathwaite, L., Folmar, G.J., 2000. Phosphorus management at the watershed scale: a modification of the phosphorus index. J. Environ. Qual. 29, 130–144.
Geohring, L.D., McHugh, O.V., Walter, M.T., Steenhuis, T.S., Akhtar, M.S., Walter, M.F., 2001. Phosphorus transport into subsurface drains by macropores after manure applications: implications for best manure management practices. Soil Sci. 166 (12), 896–909.
Harpold, A.A., Lyon, S.W., Troch, P.A., Steenhuis, T.S., 2010. Effects of preferential hydrological pathways in a glaciated watershed in the Northeastern USA. Vadose Zone J. 9, 397–414.
Hijmans, R.J., Williams, E., Vennes, C., 2012. Geosphere: Spherical Trigonometry. Package version 1., pp. 3–8, http://CRAN.R-project.org/package=geosphere
Kirchner, J.W., 2006. Getting the right answers for the right reasons: linking measurements, analyses, and models to advance the science of hydrology. Water Resour. Res. 42, W03S04, http://dx.doi.org/10.1029/2005WR004362.
Kirpich, P.Z., 1940. Time of concentration of small agricultural watersheds. Civil Eng. 10, 362.
Kleinman, P.J.A., Sharpley, A.N., McDowell, R.W., Flaten, D.N., Buda, A.R., Tao, L., Bergstrom, L., Zhu, Q., 2011. Managing agricultural phosphorus for water quality protection: principles for progress. Plant Soil 349, 169–182.
Lyne, V., Hollick, M., 1979. Stochastic time-variable rainfall-runoff modelling. IE Aust Natl Conf Publ.
Lyon, S.W., Lembo, A.J., Walter, M.T., Steenhuis, T.S., 2006. Defining probability of saturation with indicator kriging on hard and soft data. Adv. Water Resour. 29, 181–193.
Lyon, S.W., Walter, M.T., Gérard-Marchant, P., Steenhuis, T.S., 2004. Using a topographic index to distribute variable source area runoff predicted with the SCS curve-number equation. Hydrol. Process. 18, 2757–2771.
Marjerison, R.D., Dahlke, H., Easton, Z.M., Seifert, S., Walter, M.T., 2011. A phosphorus index transport factor based on variable source area hydrology for New York State. J. Soil Water Conserv. 66, 149–157.
McDowell, R.W., Srinivasan, M.S., 2009. Identifying critical source areas for water quality: 2. Validating the approach for phosphorus and sediment losses in grazed headwater catchments. J. Hydrol. 379, 68–80.
Moriasi, D.N., Arnold, J.G., Van Liew, M.W., Bingner, R.L., Harmel, R.D., Veith, T.L., 2007. Model evaluation guidelines for systematic quantification of accuracy in watershed simulations. Trans. ASABE 50, 885–900.
NOAA, 2013. NOAA – National Oceanic and Atmospheric Administration – Weather [WWW Document]. http://www.noaa.gov/wx.html (accessed 22.11.13).
NRCS, 2013. SSURGO/STATSGO2 Structural Metadata and Documentation NRCS Soils [WWW Document]. http://soils.usda.gov/survey/geography/ssurgo/ (accessed 01.11.13).
Nash, J.E., Sutcliffe, J.V., 1970. River flow forecasting through conceptual models. Part I – A discussion of principles. J. Hydrol. 10, 282–290.
Pradhan, N.R., Ogden, F.L., 2010. Development of a one-parameter variable source area runoff model for ungauged basins. Adv. Water Resour. 33, 572–584.
Priestley, C.H.B., Taylor, R.J., 1972. On the assessment of surface heat flux and evaporation using large-scale parameters. Mon. Weather Rev. 100 (2), 81–92.
R Core Team, 2013. R: A language and environment for statistical computing, Vienna, Austria.
Schneiderman, E.M., Steenhuis, T.S., Thongs, D.J., Easton, Z.M., Zion, M.S., Neal, A.L., Mendoza, G.F., Walter, M.T., 2007. Incorporating variable source area hydrology into a curve-number-based watershed model. Hydrol. Process. 21, 3420–3430.
Seibert, J., 1999. Regionalisation of parameters for a conceptual rainfall-runoff model. Agric. For. Meteorol. 98, 279–293.
Seibert, J., McGlynn, B.L., 2007. A new triangular multiple flow direction algorithm for computing upslope areas from gridded digital elevation models. Water Resour. Res. 43, W04501, http://dx.doi.org/10.1029/2006WE005128.
Shaw, S.B., Walter, M.T., 2009. Improving runoff risk estimates: formulating runoff as a bivariate process using the SCS curve number method. Water Resour. Res. 45, W03404, http://dx.doi.org/10.1029/2008WR006900.
Shuttleworth, W.J., 1992. Evaporation. In: Maidment, D.R. (Ed.), Handbook of Hydrology. McGraw-Hill, USA, pp. 4.1–4.53.
Steenhuis, T.S., Winchell, M., Rossing, J., Zollweg, J.A., Walter, M.F., 1995. SCS runoff equation revisited for variable-source runoff areas. J. Irrig. Drain. Eng. 121 (3), 234–238.
Tarboton, D.G., 1997. A new method for the determination of flow directions and upslope areas in grid digital elevation models. Water Resour. Res. 33, 309–319.
Thornthwaite, C.W., Mather, J.R., 1955. The water balance. Publ. Climatol. 8.
USDA-NRCS, 2004. National Engineering handbook (NEH), Section 4, Hydrology. US Government Press, USDA.
USDA-NRCS, 2013. Soil Data Viewer [WWW Document]. http://soildataviewer.nrcs.usda.gov/
USGS, 2013. USGS Water Data for the Nation [WWW Document]. USGS Water Data Nation http://waterdata.usgs.gov/nwis (accessed 06.12.13).
Van Steenbergen, N., Willems, P., 2013. Increasing river flood preparedness by real-time warning based on wetness state conditions. J. Hydrol. 489, 227–237.
Walter, M.T., Mehta, V.K., Marrone, A.M., Boll, J., Gérard-Marchant, P., Steenhuis, T.S., Walter, M.F., 2003. Simple estimation of prevalence of Hortonian flow in New York City watersheds. J. Hydrol. Eng. 8, 214–218.
Walter, M.T., Steenhuis, T.S., Mehta, V.K., Thongs, D., Zion, M., Schneiderman, E., 2002. Refined conceptualization of TOPMODEL for shallow subsurface flows. Hydrol. Process. 16, 2041–2046.
Walter, M.T., Walter, M.F., Brooks, E.S., Steenhuis, T.S., Boll, J., Weiler, K., 2000. Hydrologically sensitive areas: variable source area hydrology implications for water quality risk assessment. J. Soil Water Conserv. 55, 277–284.
Walter, M.T.M., Brooks, E.S., McCool, D.K., King, L.G., Molnau, M., Boll, J., 2005. Process-based snowmelt modeling: does it require more input data than temperature-index modeling? J. Hydrol. 300, 65–75.